Role of polaron hopping in leakage current behavior of a SrTiO3 single crystal

Y. Cao, S. Bhattacharya, J. Shen, C. A. Randall, and L. Q. Chen

Citation: Journal of Applied Physics **114**, 224102 (2013); doi: 10.1063/1.4842836
View online: http://dx.doi.org/10.1063/1.4842836
View Table of Contents: http://scitation.aip.org/content/aip/journal/jap/114/22?ver=pdfcov
Published by the AIP Publishing

Role of polaron hopping in leakage current behavior of a $SrTiO_3$ single crystal

Y. Cao,[1,a)] S. Bhattacharya,[2] J. Shen,[3] C. A. Randall,[1] and L. Q. Chen[1]
[1]*Department of Materials Science and Engineering, Penn State University, University Park, Pennsylvania 16802, USA*
[2]*Department of Materials Science and Engineering, Indian Institute of Technology Hyderabad, YM 502205, India*
[3]*Department of Mathematics, Purdue University, West Lafayette, Indiana 47907, USA*

(Received 4 September 2013; accepted 22 November 2013; published online 10 December 2013)

We studied the ionic/electronic transport and resistance degradation behavior of dielectric oxides by solving the electrochemical transport equations. Here, we took into account the non-periodical boundary conditions for the transport equations using the Chebyshev collocation algorithm. A sandwiched Ni|$SrTiO_3$|Ni capacitor is considered as an example under the condition of 1.0 V, 1.0 μm thickness for $SrTiO_3$ layer, and a temperature of 150 °C. The applied voltage resulted in the migration of ionic defects (oxygen vacancies) from anode towards cathode. The simulated electric potential profile at steady state is in good agreement with the recent experimental observation. We introduced the possibility of polaron-hopping between Ti^{3+} and Ti^{4+} at the electrode interface. It is shown that both the oxygen vacancy transport and the polaron-hopping contribute to the resistance degradation of single crystal $SrTiO_3$, which is consistent with the experimental observations. © *2013 AIP Publishing LLC*. [http://dx.doi.org/10.1063/1.4842836]

I. INTRODUCTION

Dielectric and ferroelectric perovskites, such as lead-zirconate titanite (PZT), strontium titanite ($SrTiO_3$), and barium titanite ($BaTiO_3$), have been widely utilized in various electronic devices such as sensors, actuators, varistors, and multilayer ceramic capacitors (MLCCs).[1] High density integration of devices and the desire for larger capacitance require ever-decreasing physical size and thickness for the dielectric layers. As a result, the reliability of these devices at reduced sizes, higher fields, and operating temperatures has become a major concern in capacitor industry.

Among all the factors that affect the lifetime of MLCCs, the long-term resistance degradation emerged as one of the most important. It is characterized by slowly increasing leakage currents under dc field stress, followed by a rapid increase of currents indicating the breakdown of capacitors (Fig. 1). Experimentally, the highly accelerated lifetime testing (HALT) has been most widely used to investigate the degradation phenomenon in dielectric and ferroelectric perovskites.[2,3]

It is well recognized that electrotransport of oxygen vacancies plays an important role in the resistance degradation, as is evidenced by the electrocoloration at the anode and cathode.[4,5] However, the role of oxygen vacancy migration in degradation is still not clear. Using High Resolution Transmission Electron Microscopy (HRTEM) and Electron Energy Loss Spectroscopy (EELS), Yang *et al.* examined the oxygen vacancy distribution after degradation and observed an increase of oxygen vacancy across the dielectric layers towards the cathode. Within each $BaTiO_3$ grain, there was a pileup of oxygen vacancies in the cathodic side and a net decrease towards the anodic side of the grain due to the blocking effects of grain boundaries.[6] Yoon *et al.* suggested that the increase of effective acceptor concentration (Mg) of $BaTiO_3$ as the grain size decreases causes high oxygen vacancy concentrations, leading to faster degradation rates.[7] Yoon also found out that the space charge polarization at grain boundaries by the charge carriers of pre-dominant holes and small portion of oxygen vacancies results in dielectric relaxation in $BaTiO_3$.[8] Despite all these works, however, due to the complexity that many factors may influence the degradation, such as acceptor doping, polarization current, dielectric layer thickness, and electrode microstructure, the key mechanism of resistance degradation has not yet been well understood experimentally.

On the other hand, mathematical models of ionic/electronic defect transport have been proposed to study current response and resistance degradation phenomenon.[9–13] Baiatu and Waser *et al.* presented mathematic models for $SrTiO_3$ single crystals and ceramics under high electric field stress.[9,10] In these models, the dielectric breakdowns were mainly attributed to the electronic compensation for oxygen vacancies accumulated near cathode ($n \approx 2[V_O^{\bullet\bullet}]$). Later, Meyer *et al.* suggested pinning of compensating electrons by the work function of the electrodes on both sides of $Ba_{0.3}Sr_{0.7}TiO_3$ thin film but did not observe any resistance

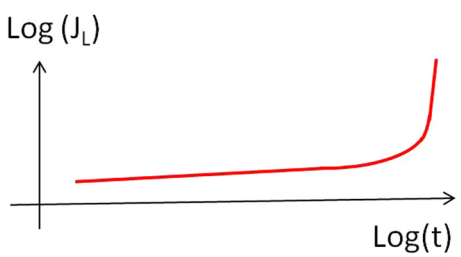

FIG. 1. Schematic plot of a typical time dependent leakage current evolution during a HALTs test.

a)Electronic mail: yxc238@psu.edu

degradation behavior.[11] More recently, a new mean time to failure (MTTF) equation was introduced by Randall *et al.* that considered critical accumulation of oxygen vacancies concentration under different field and temperatures to more accurately predict the degradation rates.[12] Strukov *et al.* provided a model of coupled drift-diffusion equations for electrons and ions and examined the mobile ion distributions and current–voltage characteristics of thin film semiconductor memristor.[13] With all of this interest in coupled electronic and ionic conduction in mixed oxide functional materials, there is a need for deeper understanding of the transient processes that occur on a local and macroscopic scale in these materials.

The main objective of this work is to explore the contribution of polaron hopping conduction[14] between Ti^{3+} and Ti^{4+} to the mechanism of resistance degradation that occurs in high concentrations of oxygen vacancies. We propose to solve the set of electrochemical transport equations using spectral method based on Chebyshev transforms along the transport direction and Fourier transforms along the plane normal to the transport direction.

II. MODEL

We chose acceptor doped $SrTiO_3$ single crystal as an example and studied the resistance degradation mechanism. The $SrTiO_3$ thin film was constrained on both sides by the Ni electrodes. The major defects of interest included the oxygen vacancies ($V_O^{\bullet\bullet}$), electrons (e'), holes ($h^{\bullet}$), polarons, and ionized acceptors (A'). The oxygen vacancies, electrons, holes, and polarons were considered as mobile species, while the ionized acceptors were assumed to be immobile. The monovalent acceptors were introduced from the substitution of +3 elements such as Fe and Al on the Ti sites (Fe'_{Ti} and $Al'_{Ti} = A'$). The reduction-oxidation reaction and the intrinsic electron-hole generation in Kröger-Vink notation were considered as major defect reactions in the current study. They are listed in Eqs. (1) and (2) with corresponding reaction constants collected from literature[9]

$$O_O = \frac{1}{2}O_2(g) + V_O^{\bullet\bullet} + 2e', \tag{1a}$$

$$K_O = [V_O^{\bullet\bullet}]n^2 p_{O_2}^{1/2} = 1.4 \times 10^{71} \exp\left(-\frac{5.18\,\text{eV}}{k_B T}\right) \text{cm}^{-9}\text{Pa}^{1/2}, \tag{1b}$$

$$\text{nil} = e' + h^{\bullet}, \tag{2a}$$

$$K_i = np = N_c N_v \exp\left(-\frac{E_g}{k_B T}\right) \text{cm}^{-6}, \tag{2b}$$

in which K_O and K_i are the chemical reaction constants, p_{O_2} is the oxygen vacancy partial pressure, N_c and N_v are the effective density of states of the conduction and valance bands in the thin film, respectively, and E_g is the band gap of single crystal $SrTiO_3$.

Due to extremely low mobility of oxygen vacancies compared to electrons and holes, they are considered to be the major factor in determining the long time dependent evolution. The oxygen vacancy migration consists of the chemical diffusion due to concentration gradient and the electrical drift under an electric field. A classic Nernst-Planck transport model has been applied to describe the oxygen vacancies migration

$$\begin{aligned} J_{V_O^{\bullet\bullet}} &= -D_{V_O^{\bullet\bullet}} \nabla [V_O^{\bullet\bullet}] + \mu_{V_O^{\bullet\bullet}} [V_O^{\bullet\bullet}] \vec{E}, \\ \frac{\partial [V_O^{\bullet\bullet}]}{\partial t} &= -\nabla \bullet J_{V_O^{\bullet\bullet}}, \end{aligned} \tag{3}$$

in which $[V_O^{\bullet\bullet}]$ is the oxygen vacancy concentration, $J_{V_O^{\bullet\bullet}}$ is the flux of the oxygen vacancy, $D_{V_O^{\bullet\bullet}}$ and $\mu_{V_O^{\bullet\bullet}}$ are the diffusivity and mobility of oxygen vacancy, respectively, which are related to each other through the Nernst-Einstein equation, $D_{V_O^{\bullet\bullet}} = (k_B T / z_{V_O^{\bullet\bullet}} e_0)\mu_{V_O^{\bullet\bullet}}$, in which k_B is the Boltzmann constant, T is the absolute temperature, $z_{V_O^{\bullet\bullet}} = +2$ denotes the effective valence for oxygen vacancy, and e_0 is the unit charge. The Ni electrodes act as the blocking boundaries for oxygen vacancies during the resistance degradation such that the boundary condition for Eq. (3) can be written as

$$J_{V_O^{\bullet\bullet}}|_{z=0,L} = 0. \tag{4}$$

$\vec{E}$ in Eq. (3) is the local electric field dependent on the charged carrier distribution. It also depends on the boundary conditions on the film surfaces. The local electric field/potential distribution is described by the Poisson equation

$$-\nabla^2 \psi = \frac{\rho}{\varepsilon_0 \varepsilon_r} = \frac{e(2[V_O^{\bullet\bullet}] + p - n - n_{polaron} - [A'])}{\varepsilon_0 \varepsilon_r}, \tag{5}$$

in which ψ is the local electric potential, ρ is the total defect charge distribution, $[V_O^{\bullet\bullet}]$, n, p, $n_{polaron}$, and $[A']$ denote the local concentration of oxygen vacancy, electron, hole, polaron, and ionized acceptors, respectively. The electric potential ψ is related to the electric field through $\vec{E} = -\nabla\psi$. The boundary condition for the electric potential is defined as

$$\psi|_{z=0} = V_a(0) + \eta, \quad \psi|_{z=L} = V_a(L) - \eta, \tag{6}$$

in which $V_a(0)$ and $V_a(L)$ are the applied potential bias at $z = 0, L$. η is the overpotential of the electrochemical reaction occurred at the metal/semiconductor interface.

On the other hand, electrons and holes are moving much faster than oxygen vacancies due to their higher mobility. In our simulation, we assume that the electronic species always reach equilibrium for each concentration evolution of oxygen vacancy profile. The transport of electrons and holes are described in the following equations:

$$\begin{aligned} J_n &= -D_n \nabla n - \mu_n n \vec{E}, \\ \frac{\partial n}{\partial t} &= -\nabla \bullet J_n = D_n \nabla^2 n + \mu_n \nabla \bullet [n\vec{E}] = 0, \end{aligned} \tag{7}$$

$$\begin{aligned} J_p &= -D_p \nabla p + \mu_p p \vec{E}, \\ \frac{\partial p}{\partial t} &= -\nabla \bullet J_p = D_p \nabla^2 p - \mu_p \nabla \bullet [p\vec{E}] = 0. \end{aligned} \tag{8}$$

The electron and hole concentrations at the Ni/$SrTiO_3$ interface are pinned by the Ni electrode as

$$n_{z=0,L} = N_c \exp\left(-\frac{E_c - E_{fm}}{k_B T}\right), \tag{9}$$

$$p_{z=0,L} = N_V \exp\left(-\frac{E_{fm} - E_v}{k_B T}\right). \tag{10}$$

The energy of the conduction band (E_c) and valence band (E_v) and the work function of the metal electrode (E_{fm}) are listed in Table I.

We proposed a polaron hopping conduction model to study its effect on the leakage current evolution. The polarons were treated as localized monovalent charge carriers and they contribute to the total current by hopping between Ti^{3+} and Ti^{4+} sites, i.e., $Ti^{4+} + e^- = Ti^{3+}$. A schematic plot of the polaron hopping model is shown in Fig. 2. The flux of polarons at the cathode ($Ti^{4+} + e^- = Ti^{3+}$) is described by the so called Butler-Volmer equation

$$\begin{aligned} J_{cathode} &= J_{f(cathode)} - J_{b(cathode)} \\ &= k_+ c_{Ti^{4+}} \exp\left[\frac{(1-\beta)nF}{RT}\eta\right] - k_- c_{Ti^{3+}} \exp\left[\frac{-\beta nF}{RT}\eta\right], \end{aligned} \tag{11}$$

in which $c_{Ti^{4+}}$ and $c_{Ti^{3+}}$ are the local concentration of Ti^{4+} and Ti^{3+}, respectively, k_+ and k_- are the forward and backward reaction rate constants, β is the transfer coefficient, and η is the overpotential of the reaction. Similarly, the flux of polaron at the anode ($Ti^{3+} = Ti^{4+} + e^-$) is written as

$$\begin{aligned} J_{anode} &= J_{f(anode)} - J_{b(anode)} \\ &= k_+ c_{Ti^{3+}} \exp\left[\frac{-\beta nF}{RT}\eta\right] - k_- c_{Ti^{4+}} \exp\left[\frac{(1-\beta)nF}{RT}\eta\right]. \end{aligned} \tag{12}$$

The electrotransport of polarons follows a diffusion equation with the boundary conditions determined by the flux which is given in Eqs. (11) and (12).

The current density is determined from the flow of the charged species of oxygen vacancies, electrons, holes, and polarons. Ionized acceptors are assumed to be immobile so that they do not contribute to the current density. The current density for particular charged carrier i and the total current density are given by

TABLE I. Parameters for the simulation.

Parameter	Value	Parameter	Value
p_{O_2}	0.1 Pa	$[A']$	$2.0 \times 10^{18}\,cm^{-3}$
E_C	−4.0 eV	$\mu_{V_O^{\cdot\cdot}}$	$1.0 \times 10^{-9} cm^2 \cdot V^{-1} \cdot s^{-1}$
E_V	−7.0 eV	μ_n	$1.6\ cm^2 \cdot V^{-1} \cdot s^{-1}$
E_g	3.0 eV	μ_p	$0.8\ cm^2 \cdot V^{-1} \cdot s^{-1}$
E_{fm}	−5.3 eV	$\mu_{polaron}$	$0.01\ cm^2 \cdot V^{-1} \cdot s^{-1}$
L	1.0 μm	β	0.5
ε_r	150	η	0.1 V

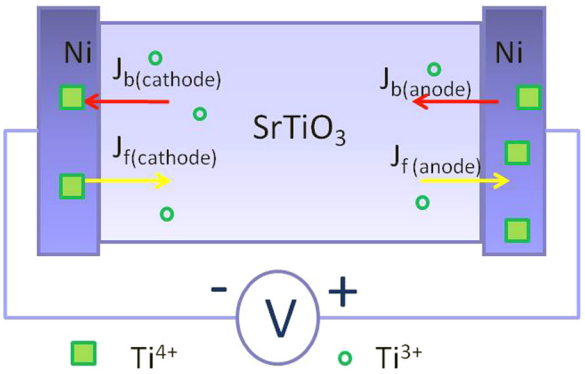

FIG. 2. Schematic plot of the Ni|$SrTiO_3$|Ni sandwich structure and the small polaron hopping between Ti^{3+} and Ti^{4+} ($Ti^{4+} + e^- = Ti^{3+}$).

$$I_i = e_0 z_i J_i, \tag{13}$$

$$I_{total} = \sum_i I_i, \tag{14}$$

in which i denote oxygen vacancy, electron, hole, or polaron.

III. RESULTS AND DISCUSSION

We considered $SrTiO_3$ single crystal as an example relative to a single dielectric layer oriented to the normal of the electrode plates. We set up a coordinate system with periodic boundary condition along x and y directions. Along z direction, it is non-periodic so that a Chebyshev collocation boundary condition was applied. Initially, we were mainly concerned with the ionic/electronic transport along z direction. Therefore, the system size of the simulation was chosen to be $1 \times 1 \times 200$.

To solve the above equations, the semi-implicit Fourier-spectral method was employed.[15] Considering the time dependent transport [Eq. (3)], more generally, we rewrite it as

$$\frac{\partial C(r,t)}{\partial t} = D\nabla^2 C(r,t) - \mu\nabla\bullet[C(r,t)\vec{E}], \tag{15}$$

in which $C(r,t)$ is the concentration of the diffusant and the diffusivity D is assumed to be space independent. Solving the above equation with a finite difference or Fourier approximation in space has a severe time step limit of $\Delta t \le \lambda/N^2$ where λ is a constant and N is the number of lattice points in each space dimension. To avoid this limitation, a semi-implicit treatment is considered. From Eq. (15), we have

$$\begin{aligned} \frac{C^{n+1} - C^n}{\Delta t} &= D\nabla^2 C^{n+1} - \mu\nabla\bullet[C^n\vec{E}], \\ \frac{C^{n+1}}{D\Delta t} - \nabla^2 C^{n+1} &= \frac{C^n}{D\Delta t} - \left(\frac{\mu}{D}\right)\nabla\bullet[C^n\vec{E}], \end{aligned} \tag{16}$$

write $u = C^{n+1}$, $\alpha = 1/(D\Delta t)$, and $f = C^n/(D\Delta t) - (\mu/D)\nabla\bullet[C^n\vec{E}]$, Eq. (16) can be simplified as

$$\alpha u - \nabla^2 u = f, \tag{17}$$

with periodic boundary condition along x and y directions and a non-periodic boundary condition along z direction. At

each time step, Eq. (17) can be accurately solved using Chebyshev collocation algorithm. Details of this algorithm are described in the Appendix.

We started with a charge neutral single crystal $SrTiO_3$ with film thickness $L = 1\,\mu$m of acceptor doping concentration $[A'] = 2.0 \times 10^{18}\text{cm}^{-3}$. The simulation condition and the parameters of the material are listed in Table I. We first performed the simulation of charge transport without taking into account the polaron hopping conduction. The initial charged defect concentrations were assumed to be homogeneous and calculated based on the defect chemical reaction (Eqs. (1) and (2)) and the local neutrality condition, with monovalent acceptors mainly compensated by the oxygen vacancies

$$2[V_O^{\bullet\bullet}] + p - n - [A'] = 0. \tag{18}$$

The simulation was then performed at $T = 1000\,\text{K}$ with $p_{O_2} = 0.1\text{Pa}$ to simulate the annealing process of the sample with Ni electrodes at elevated temperature. The oxygen vacancy concentrations at the metal/dielectric interfaces were determined from Eq. (1b)

$$[V_O^{\bullet\bullet}]|_{z=0,L} = \frac{K_O}{n_{z=0,L}^2 p_{O_2}^{1/2}}, \tag{19}$$

in which $n_{z=0,L}$ is the electron concentration at the interface which is assumed to be pinned by the work function of metal electrodes (Eqs. (9) and (10)). By numerically solving the coupled equations (Eqs. (3), (5), (7), and (8)) with appropriate boundary conditions (Eqs. (6), (9), (10), and (19)), we obtained the equilibrium profiles of space charges and interior electric potential for the initial unbiased condition as shown in Fig. 3. From Fig. 3(a), it can be seen that the thin film remained charge neutral. In the vicinity of the $Ni/SrTiO_3$ interfaces, however, negatively charged layers were formed with enrichment of electrons and depletion of oxygen vacancies and holes. An upward bending electric potential profile was formed in response to the ionic and electronic redistribution (Fig. 3(b)).

After the charged defects and electric potential distribution reached equilibrium, the resistance degradation simulation was implemented by applying an external potential bias of 1.0 V on the sample at $T = 150\,^\circ\text{C}$. At low temperature, the Ni electrodes acted as blocking boundaries for oxygen vacancies transport (Eq. (4)) so that the total oxygen vacancies remained constant. Electron and hole concentrations at the interfaces were still pinned by the Ni electrodes (Eqs. (9) and (10)). Fig. 4 shows the evolution profiles of charged defects and electric potential, with cathode on the left side ($z = 0$, $\psi = 0$) and anode on the right hand side ($z = L, \psi = 1.0\text{V}$). In Fig. 4(a), the oxygen vacancies tended to migrate towards the cathode under the electric field, resulting in a net positive charge layer near cathode and negative charge layer near anode. On the other hand, electrons and holes tended to redistribute to compensate the net charges induced from oxygen vacancy segregation and depletion (Figs. 4(b) and 4(c)). It should be noted that the electronic charge compensation was limited based on the assumption that electronic defect

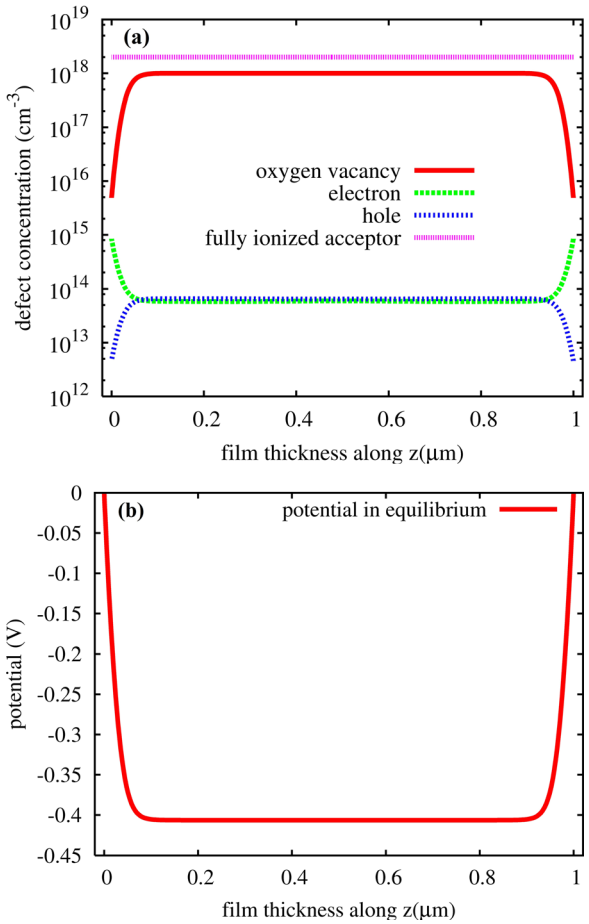

FIG. 3. The ionic/electronic charged defects and inner potential distribution in equilibrium $SrTiO_3$ single layer of 1 μm in thickness at $T = 1000\,\text{K}$ (with no external applied potential bias). (a) oxygen vacancy, electron, hole, and fully ionized acceptors; (b) inner potential profile.

concentrations at the metal/dielectric interfaces were pinned by the work function of the metal electrodes. The electric potential distribution at steady state was almost constant inside the thin film and near cathode region due to charge screening. However, it exhibited a large gradient near anode side, indicating a locally concentrated electric field along $-z$ direction (Fig. 4(d)). This is due to the ionic depletion in the vicinity of the anode. Our simulation result is consistent with recent experimental work by Okamoto *et al.* in which a highly concentrated electric field along anode side was observed in the degraded MLCCs.[16]

The leakage current evolution under an electric field was studied and plotted in Fig. 5. It is seen that the current density experienced a small increase in the initial stage ($t < 10\,\text{s}$) until it reached constant and no longer changed with time. The net current density increase was below one order of magnitude and thus there was no resistance degradation phenomenon in single crystal $SrTiO_3$ under the current simulation condition. In our current model, we pinned the boundary concentrations of electronic defects based on the Fermi level of the metallic electrode, and thus limited the electronic contribution to the leakage current. Our result showing no degradation in acceptor doped $SrTiO_3$ single crystal is different from what was previously reported,[9] that the current density increased

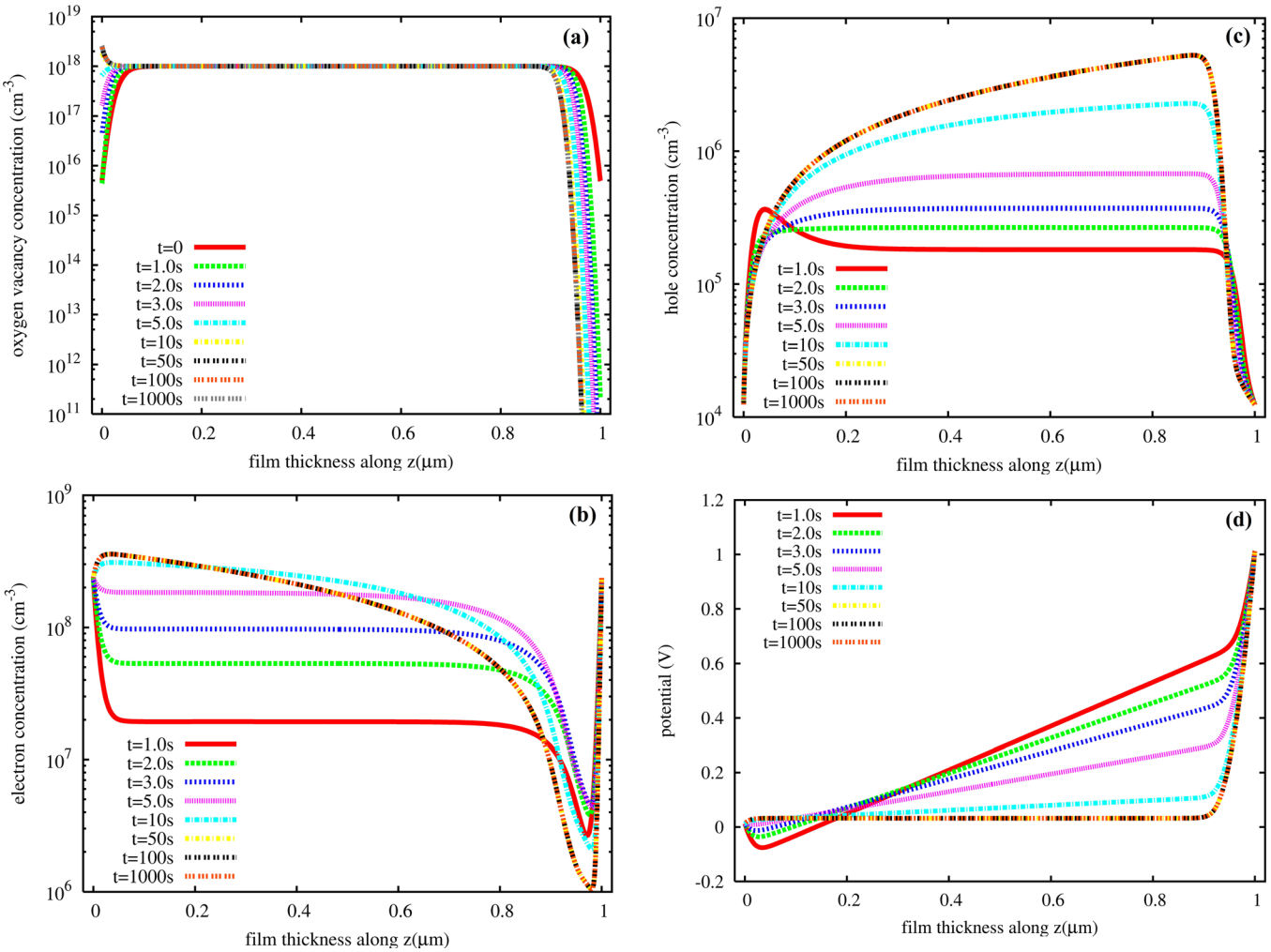

FIG. 4. Evolution of charged defects and electric potential profile to steady state for $SrTiO_3$ at $T = 150\,^{\circ}C$ under a 1.0 V external bias (a) oxygen vacancy; (b) electron; (c) hole, and (d) electric potential profile.

by at least one order of magnitude due to the dramatic increase in the electron concentration near the cathode, $\sim 10^{18}\,cm^{-3}$, to compensate the segregated oxygen vacancy in that region. However, our result agrees with more recent work on dc current response of a $Ba_{0.3}Sr_{0.7}TiO_3$ thin film capacitor by Meyer *et al.*,[11] who showed that there was no resistance degradation also based on the assumption that the electron concentration at the electrode/dielectric interfaces is pinned by the electrodes.

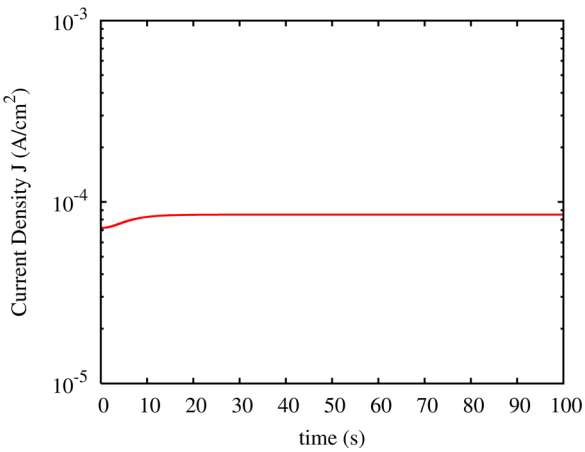

FIG. 5. Calculated time-dependent leakage current evolution under 1.0 V dc bias at 150 °C.

The fact that real dielectric capacitors' display degradation indicates that there must be other aspects to the total degradation mechanism. Recently, a small polaron hopping conduction was suggested as a possible mechanism for the dielectric degradation phenomenon.[14] The main objective of this work is to test the hypothesis that polaron hopping makes important contribution to the leakage current evolution. The temporal profiles of polaron evolution were obtained by solving the diffusion equation using boundary conditions (11) and (12). The initial polaron concentration in $SrTiO_3$ was estimated to be $10^{14}\,cm^{-3}$ based on literature.[17] From Fig. 6, the polaron concentration started to increase at the cathode side, due to a net flow of electrons from cathode into the dielectric layer. The polaron concentration reached $\sim 10^{17}\,cm^{-3}$ in compensation to the excess of positive charges due to the oxygen vacancy segregation at the cathode side (Fig. 4(a)). In the anode region, the polaron concentration decreased for charge balance due to the significant oxygen vacancy depletion in the anode region (Fig. 4(a)). Our simulation result was evidenced by the recent experiment, in which a high local polaron concentration was observed in the degraded cathode region of a 1% Fe-doped

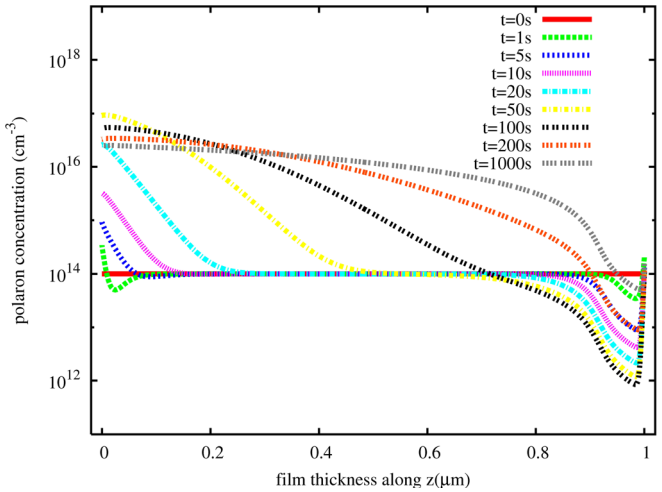

FIG. 6. Evolution of polaron under flux boundary condition in $SrTiO_3$ under 1.0 V dc bias.

single crystal $SrTiO_3$.[14] The simulated polaron concentration in cathode was two orders of magnitude lower than that in paper of Liu *et al.*[14] This is because of a much higher doping concentration (~1%) in their experiments, which result in the oxygen vacancy accumulation up to 10^{20} cm^{-3}.

The current density evolution, which takes into account the polaron hopping conduction, is shown in Fig. 7. The leakage current density remained low in the initial time range (<10 s) and increased significantly at ~10 s, when oxygen vacancies, free electrons, and polarons tended to segregate at the cathode side. As pointed out by Meyer *et al.*,[11] the transport of oxygen vacancies and the ionic conduction itself does not fully explain the degradation process. Based on our simulation, the increase of ionic current was limited (Fig. 5), and the contribution of free electronic electrons to the leakage current was negligible due to extreme low electronic concentration, the leakage current increase by more than one order of magnitude could be explained by the local polaron hopping conduction. This was further evidenced by the correlation between the polaron concentration in cathode and leakage current density in the process of resistance degradation. It is seen from Fig. 8 that the calculated polaron

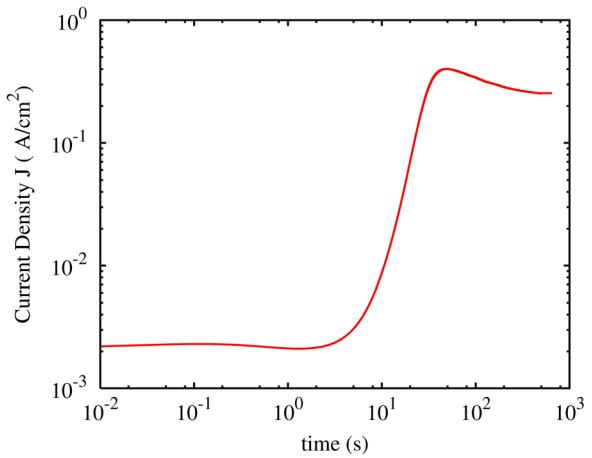

FIG. 7. Calculated leakage current evolution considering the small polaron hopping conduction mechanism under 1.0 V dc bias at 150 °C.

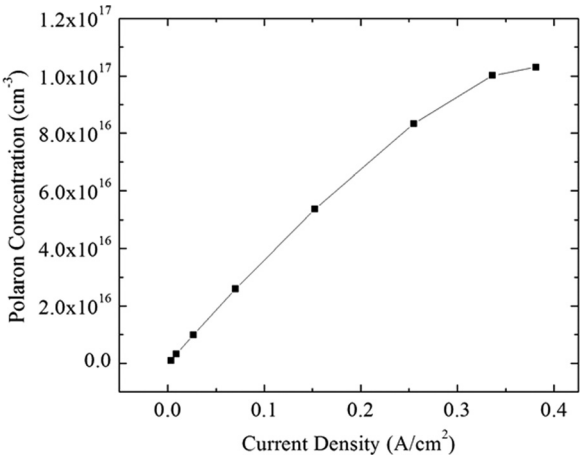

FIG. 8. Calculated polaron concentration in cathode vs. leakage current density in the resistance degradation process (from 5 to 40 s with 5 s interval).

concentration increased with the degree of degradation. This agrees with Liu's experimental results.[14] Therefore, it can be suggested that the polaron hopping conduction should be considered as a possible mechanism for the resistance degradation behavior in single crystal $SrTiO_3$ and other dielectrics.

IV. SUMMARY

In this paper, we studied the resistance degradation behavior of acceptor doped $SrTiO_3$ single crystal by solving the coupled defect transport and Poisson equations using Chebyshev Collocation Algorithm. Our simulation successfully showed the ionic and electronic transport under external field and the steady state profile of electric potential, which is consistent with the recent experimental result. Our simulation showed no resistance degradation behavior based on the assumption that the electronic defects are pinned by the work function of metal electrodes at the interfaces. This agrees with the recent work by Meyer *et al*. Finally, by introducing the polaron hopping between Ti^{3+} and Ti^{4+} into the current model, we successfully modeled leakage current behavior and suggest that the resistance degradation phenomenon in dielectric capacitors can possibly be explained by the polaron hopping conduction. In the future, we will incorporate the ferroelectric domain structure and study the coupling behaviors between space charges and polarization to understand their effect on the resistance degradation in ferroelectric capacitors.

ACKNOWLEDGMENTS

The authors are grateful to the financial support for NSF-IUCRC Center for Dielectric Studies at Penn State. The work of Jie Shen is partially supported by NSF DMS-1215066 and by the Computational Materials and Chemical Sciences Network (CMCSN)

APPENDIX: CHEBYSHEV COLLOCATION ALGORITHM

We introduced the Chebyshev collocation method to solve the second-order partial differential equation

$$\varepsilon u''(x) + p(x)u'(x) + q(x)u(x) = f(x) \text{ in } (-1,1)^2, \quad \text{(A1)}$$

where ε is a fixed parameter and $p(x)$, $q(x)$, and $f(x)$ are the given functions. The boundary condition for Eq. (A1) is given by

$$\begin{aligned} a_- u(-1) + b_- u'(-1) &= c_-, \\ a_+ u(+1) + b_+ u'(+1) &= c_+. \end{aligned} \quad \text{(A2)}$$

We first consider the Dirichlet boundary condition

$$u(-1) = c_-, \quad u(+1) = c_+. \quad \text{(A3)}$$

The Chebyshev interpolation polynominal can be written as

$$u^N(x) = \sum_{j=1}^{n} U_j F_j(x), \quad \text{(A4)}$$

where $x_j = \cos(j\pi/N)$, $0 \le j \le N$ are the Chebyshev-Gauss-Lobatto collocation points, U_j are the unknown coefficients to be determined, and $F_j(x)$ is the Lagrange interpolation polynominal associated with $\{x_j\}$. The Chebyshev collocation method is to seek u^N in the form of Eq. (A4) such that $u^N(-1) = c_-$, $u^N(+1) = c_+$ and Eq. (18) holds at the interior collocation points

$$\varepsilon u^N_{xx}(x_j) + p(x_j)u^N_x(x_j) + q(x_j)u^N(x_j) = f(x_j), \quad i \le j \le N-1. \quad \text{(A5)}$$

By using the definition of the differentiation matrix (details can be found in Ref. 15), we obtain a set of linear equations

$$\begin{aligned} \sum_{j=1}^{N-1} \left[\varepsilon(D^2)_{ij} + p(x_i)(D^1)_{ij} + q(x_i)\delta_{ij}\right] U_j \\ = f(x_i) - \left[\varepsilon(D^2)_{i0} + p(x_i)(D^1)_{i0}\right] c_+ \\ - \left[\varepsilon(D^2)_{iN} + p(x_i)(D^1)_{iN}\right] c_-, \end{aligned} \quad \text{(A6)}$$

for the $\{U_j\}_{j=1}^{N-1}$, in which δ_{ij} is the Kronecker delta. To summarize, the spectral-collocation solution for Eq. (A1) with Dirichlet boundary conditions Eq. (A3) satisfies the linear system

$$A\bar{U} = \bar{b}, \quad \text{(A7)}$$

where $\bar{U} = [U_1, ..., U_{N-1}]^T$, the matrix $A = (a_{ij})$, and the vector $\bar{b}$ are given by

$$\begin{aligned} a_{ij} &= \varepsilon(D^2)_{ij} + p(x_i)(D^1)_{ij} + q(x_i)\delta_{ij}, \quad 1 \le i,j \le N-1, \\ b_i &= f(x_i) - \left[\varepsilon(D^2)_{i0} + p(x_i)(D^1)_{i0}\right] c_+ \\ &\quad - \left[\varepsilon(D^2)_{iN} + p(x_i)(D^1)_{iN}\right] c_-, \quad 1 \le i \le N-1. \end{aligned} \quad \text{(A8)}$$

The solution to the above system gives the approximate solution to Eqs. (A1) and (A3) at the collocation points. For general boundary conditions, the procedure is similar. The details of the solution can be found in Ref. 18.

[1] O. Auciello, J. F. Scott, and R. Ramesh, Phys. Today **51**(7), 22 (1998).
[2] W. Liu and C. A. Randall, J. Am. Ceram. Soc. **91**, 3245 (2008).
[3] W. Liu and C. A. Randall, J. Am. Ceram. Soc. **91**, 3251 (2008).
[4] H. I. Yoo, M. W. Chang, T. S. Oh, C. E. Lee, and K. D. Becker, J. Appl. Phys. **102**, 093701 (2007).
[5] R. Waser, T. Baiatu, and K. H. Hardtl, J. Am. Ceram. Soc. **73**, 1654 (1990).
[6] G. Y. Yang, G. D. Lian, E. C. Dickey, C. A. Randall, D. E. Barber, P. Pinceloup, M. A. Henderson, R. A. Hill, J. J. Beeson, and D. J. Skamser, J. Appl. Phys. **96**, 7500 (2004).
[7] S. H. Yoon, C. A. Randall, and K. H. Hur, J. Am. Ceram. Soc. **92**, 2944 (2009).
[8] S. H. Yoon, S. H. Kwon, and K. H. Hur, J. Appl. Phys. **109**, 084117 (2011).
[9] T. Baiatu, R. Waser, and K. H. Hardtl, J. Am. Ceram. Soc. **73**, 1663 (1990).
[10] T. Holbling, N. Soylemezoglu, and R. Waser, J. Electroceram. **9**, 89 (2002).
[11] R. Meyer, R. Liedtke, and R. Waser, Appl. Phys. Lett. **86**, 112904 (2005).
[12] C. A. Randall, R. Maier, W. Qu, K. Kobayashi, K. Morita, Y. Mizuno, N. Inoue, and T. Oguni, J. Appl. Phys. **113**, 014101 (2013).
[13] D. B. Strukov, J. L. Borghetti, and R. S. Williams, Small **5**, 1058 (2009).
[14] W. Liu, G. Y. Yang, and C. A. Randall, Jpn. J. Appl. Phys., Part 1 **48**, 051404 (2009).
[15] L. Q. Chen and J. Shen, Comp. Phys. Commun. **108**, 147 (1998).
[16] T. Okamoto, S. Kitagawa, N. Inoue, and A. Ando, Appl. Phys. Lett. **98**, 072905 (2011).
[17] S. Zhao, S. J. Zhang, W. Liu, N. J. Donnelly, Z. Xu, and C. A. Randall, J. Appl. Phys. **105**, 053705 (2009).
[18] J. Shen and T. Tang, *Spectral and High-Order Methods with Applications* (Science Press, Beijing, China, 2006).